The EMBO Journal Vol. 21 No. 3 pp. 314–323, 2002

A 'three-pronged' binding mechanism for the SAP/SH2D1A SH2 domain: structural basis and relevance to the XLP syndrome

Peter M.Hwang[1], Chengjun Li[2], Massimo Morra[3], Jennifer Lillywhite[2], D.Ranjith Muhandiram[1,4], Frank Gertler[5], Cox Terhorst[3], Lewis E.Kay[1,4,6], Tony Pawson[4,7], Julie D.Forman-Kay[1,8] and Shun-Cheng Li[2,9]

Departments of [1]Biochemistry, [6]Chemistry and [4]Molecular and Medical Genetics, University of Toronto, Toronto, Ontario M5S 1A8, [2]Department of Biochemistry, Faculty of Medicine and Dentistry, University of Western Ontario, London, Ontario N6A 5C1, [7]Samuel Lunenfeld Research Institute, Mt Sinai Hospital, Toronto, Ontario M5G 1X5, [8]Program in Structural Biology and Biochemistry, The Hospital for Sick Children, Toronto, Ontario M5G 1X8, Canada, [3]Division of Immunology, Beth Israel Deaconess Medical Center, Harvard Medical School, Boston, MA 02215 and [5]Department of Biology, Massachusetts Institute of Technology, 77 Massachusetts Avenue, Cambridge, MA 02139, USA

[9]Corresponding author
e-mail: sli@uwo.ca

The SH2 domain protein SAP/SH2D1A, encoded by the X-linked lymphoproliferative (XLP) syndrome gene, associates with the hematopoietic cell surface receptor SLAM in a phosphorylation-independent manner. By screening a repertoire of synthetic peptides, the specificity of SAP/SH2D1A has been mapped and a consensus sequence motif for binding identified, T/S-x-x-x-x-V/I, where x represents any amino acid. Remarkably, this motif contains neither a Tyr nor a pTyr residue, a hallmark of conventional SH2 domain–ligand interactions. The structures of the protein, determined by NMR, in complex with two distinct peptides provide direct evidence in support of a 'three-pronged' binding mechanism for the SAP/SH2D1A SH2 domain in contrast to the 'two-pronged' binding for conventional SH2 domains. Differences in the structures of the two complexes suggest considerable flexibility in the SH2 domain, as further confirmed and characterized by hydrogen exchange studies. The structures also explain binding defects observed in disease-causing SAP/SH2D1A mutants and suggest that phosphorylation-independent interactions mediated by SAP/SH2D1A likely play an important role in the pathogenesis of XLP.
Keywords: immunodeficiency/SAP/SH2 domain/SH2D1A/XLP

Introduction

X-linked lymphoproliferative (XLP) syndrome, also known as Duncan's disease, is a rare inherited immunodeficiency condition characterized by benign or malignant proliferation of lymphocytes, histiocytosis and alterations in serum immunoglobulin concentrations (Purtilo *et al*., 1975, 1978). The gene altered in XLP has recently been identified (Coffey *et al*., 1998; Nichols *et al*., 1998; Sayos *et al*., 1998). It encodes a small protein of 128 amino acids (variously named SAP, SH2D1A and DSHP), consisting of a five amino acid N-terminal sequence, an SH2 domain and a 25 residue C-terminal tail. A number of SAP/SH2D1A mutations have been identified in XLP patients (Nichols *et al*., 1998; Sayos *et al*., 1998; Yin *et al*., 1999; Sumegi *et al*., 2000) and these fall into three broad categories: (i) micro/macro-deletions that lead to a complete or partial loss of the gene; (ii) mutations that interfere with mRNA transcription or splicing; and (iii) nonsense mutations that result in premature termination of protein synthesis or missense mutations that give rise to substitution of an amino acid conserved between the human and murine SAP/SH2D1A proteins (Morra *et al*., 2001a). The missense mutations are particularly interesting since, except for one case where a stop codon at the C-terminus of the protein is replaced by that for an Arg, all the other mutations occur within the boundaries of the SH2 domain of the protein and therefore directly implicate the SH2 domain in the pathogenesis of XLP.

Although mRNA analysis has strongly linked the SAP/SH2D1A gene to XLP, little is known about the molecular mechanism of the disease at the protein level. Since SAP/SH2D1A lacks an effector domain (e.g. a catalytic domain), it was suggested to function as an inhibitor of other SH2 domain-mediated interactions in T and natural killer (NK) cells so as to enhance or prolong the activities of these cells (Satterthwaite *et al*., 1998; Sayos *et al*., 1998). In line with this possibility, SAP/SH2D1A was found to bind to the cytoplasmic domain of the hematopoietic surface receptor known as the signaling lymphocyte activation molecule (SLAM), a glycosylated transmembrane protein also known as CD150 (Cocks *et al*., 1995). This interaction, mediated by the SAP/SH2D1A SH2 domain and a tyrosine phosphorylation site (Tyr281 in SLAM), was further shown to block the recruitment of an SH2 domain-containing tyrosine phosphatase Shp2 to the same site in SLAM (Sayos *et al*., 1998). Intriguingly, SAP/SH2D1A associated with SLAM regardless of the phosphorylation state of Tyr281, indicating that its SH2 domain possesses a novel binding specificity, which raises questions about the role of tyrosine phosphorylation in SAP/SH2D1A function. An analogous complex was also documented between SAP/SH2D1A and 2B4, an activating NK cell receptor that shares significant sequence identity with SLAM (Tangye *et al*., 1999, 2000). Moreover, engagement of 2B4 by SAP/SH2D1A prevented its association with Shp2. It is, therefore, likely that SAP/SH2D1A plays similar roles in regulating the activities of T cells (via SLAM) and NK cells (via 2B4). However, contrary to the above observations, binding of SAP/SH2D1A was recently shown to be necessary to

induce tyrosine phosphorylation of SLAM by facilitating the recruitment of the Src-related tyrosine kinase FynT, rather than displacing a phosphotyrosine phosphatase (PTP) that interferes with SLAM signal transduction (Latour *et al*., 2001).

Previously, we employed a series of truncated peptides derived from sequences flanking Tyr281 in SLAM to investigate the specificity of the SAP/SH2D1A SH2 domain (Li *et al*., 1999). Results demonstrated that this SH2 domain is not only capable of binding to a pTyr residue that is followed by a stretch of C-terminal amino acids in a manner akin to that of a conventional SH2 domain, but it is also capable of recognizing a pTyr residue preceded by an N-terminal fragment or an unphosphorylated Tyr residue embedded within an appropriate sequence context. Based on these observations, a 'three-pronged plug that engages three binding sites' model was put forward to account for the tripartite nature of the SAP/SH2D1A–SLAM-Tyr281 peptide interaction (Li *et al*., 1999). This model is consistent with the crystal structures of the SAP/SH2D1A SH2 domain in a complex with two SLAM-Tyr281 peptides, one containing a pTyr residue and the other Tyr, which demonstrated that, in addition to residues C-terminal to the pTyr/Tyr, those N-terminal are also involved in binding to the SH2 domain (Poy *et al*., 1999). Here, we present two solution structures of this protein: one in complex with a peptide that lacks the entire sequence C-terminal to pTyr281 and the other with an unphosphorylated SLAM peptide. These structures provide compelling evidence in support of a 'three-pronged' mechanism for peptide recognition by the SAP/SH2D1A SH2 domain, which is further supported by results obtained from a SPOTs (Frank and Doring, 1988; Blankenmeyer-Menge *et al*., 1990) peptide binding study demonstrating that SAP/SH2D1A binds selectively to peptides with a consensus sequence motif T/S-x-x-x-x-V/I, where x denotes any amino acid. The structures, together with amide hydrogen exchange rates measured by NMR spectroscopy, also provide a rationale for the reduced binding affinities for both the phosphorylated and unphosphorylated SLAM-Y281 peptides observed for disease-causing SAP/SH2D1A missense mutants.

Results

The SAP/SH2D1A SH2 domain binds to peptide motifs containing no tyrosine

In order to determine the specificity of the SAP/SH2D1A SH2 domain in a more comprehensive manner than previously reported (Li *et al*., 1999), we synthesized a set of undecamer peptides using the SPOTs method of simultaneous multiple peptide synthesis on a derivatized cellulose membrane (Frank and Doring, 1988; Blankenmeyer-Menge *et al*., 1990). These peptides are based on the sequence of the Tyr281 site in SLAM (KSLTIYAQVQK), which contains five amino acids each at the N- and C-terminus of the Tyr281 residue and is thus designated n-Y-c for simplicity. Specifically, each position in peptide n-Y-c was permutated to allow for a full representation of all 20 naturally occurring amino acids at that position, generating a total of $11 \times 20 = 220$ spots on a cellulose membrane. A series of truncated peptides with decreasing N- or C-terminal length was also synthesized,

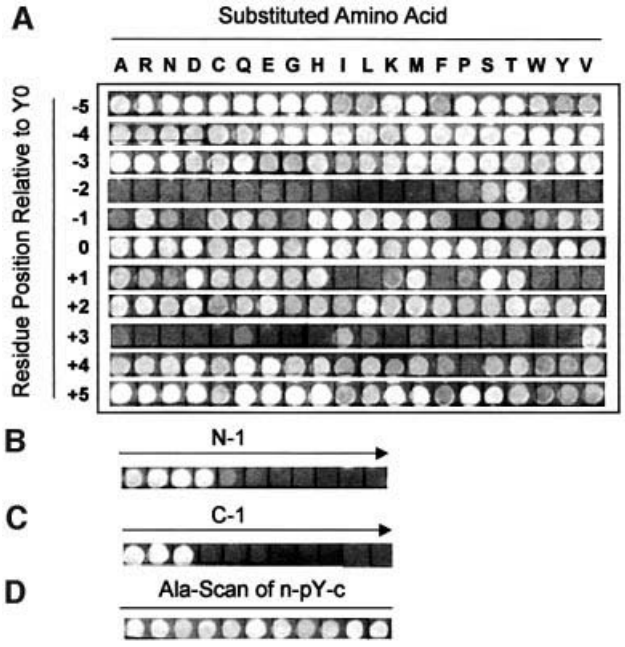

Fig. 1. Mapping the specificity of the SAP/SH2D1A SH2 domain using peptide SPOTs synthesized on cellulose membranes. The amino acid at each position of peptide n-Y-c, KSLTIYAQVQK, was permutated to all 20 naturally occurring amino acids while maintaining the sequence of the remainder of the peptide (**A**). N-1 and C-1 represent a series of peptides with progressive (one residue at a time) N- and C-terminal sequence truncations of peptide n-Y-c, respectively (**B** and **C**). Ala-scanning substitutions were carried out in the background of peptide n-pY-c, KSLTIpYAQVQK (**D**).

as was a group of Ala-scanning peptides derived from peptide n-pY-c, the phosphorylated version of peptide n-Y-c (Figure 1).

The peptide spots on the cellulose membrane were then screened for their ability to bind to purified glutathione *S*-transferase (GST)–SAP/SH2D1A. Results from the screen are displayed in Figure 1, where bright (fluorescent) spots indicate positive binding of the corresponding peptides to the protein and dark spots denote weak or negative binding. To facilitate analysis of the results, each residue in peptide n-Y-c was assigned a number according to its position relative to the central Tyr, which was given a value '0' (Figure 1). As seen in Figure 1A, residues in the peptide do not play equal roles in binding to SAP/SH2D1A. While positions +4, +5, and –3 to –5, corresponding to the extreme N- and C-termini of the peptide, and position +2 could be substituted by almost any residue without adversely affecting binding, SAP/SH2D1A is highly selective for positions –2 and +3. Binding is facilitated by residues with a hydroxyl side chain, such as Thr and Ser at position –2, and residues with hydrophobic, β-branched side chains such as Val and Ile are favored at position +3. A certain degree of selectivity was also seen at positions –1 and +1. While position –1 demonstrated a proclivity for residues with large side chains, position +1 displayed a bias against bulky, hydrophobic residues. Interestingly, there is no apparent discrimination at position 0, corresponding to the central Tyr residue in peptide n-Y-c, suggesting that within the context of the full-length peptide, the Tyr residue is completely dispens-

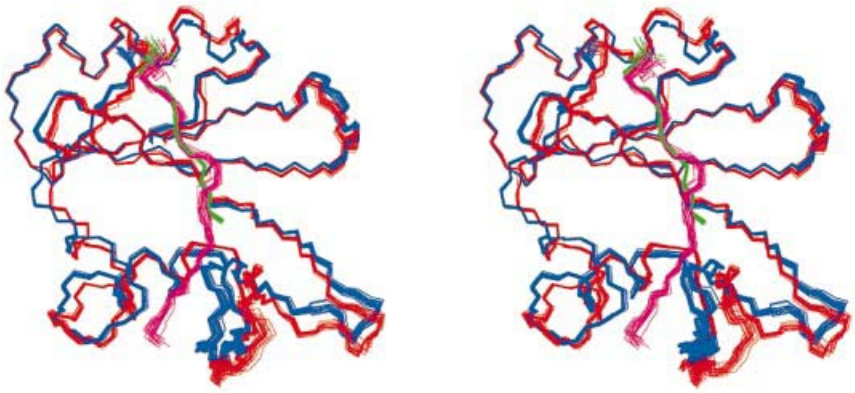

Fig. 2. Stereoview of a superposition of the 20 lowest energy structures of SAP/SH2D1A–SLAM peptide complexes (using backbone atoms of residues 6–56). The protein (residues 6–104) is shown in blue for the n-pY complex and in red for the n-Y-c complex. Peptide n-pY is depicted in green (only residues –4 to +1 relative to the pTyr are shown) and n-Y-c in magenta (only residues –4 to +5 are shown).

able for binding. It should be pointed out that GST alone did not show detectable binding to any of the peptide spots (data not shown). Collectively, these data demonstrate that SAP/SH2D1A selectively binds to a peptide motif containing the consensus sequence T/S-x-x-x-x-V/I.

The importance of residues at positions –2 and +3 is also reflected by the N- and C-terminally truncated peptides. As shown in Figure 1B, residues at the –5 to –3 positions could be deleted without compromising the affinities of the resulting peptides. However, as soon as the peptide was shortened to exclude Thr at position –2, its affinity for SAP/SH2D1A was lost. Similarly, when the C-terminal truncation reached residue Val+3, the resulting peptide was no longer active (Figure 1C). The role of a pTyr residue in binding to SAP/SH2D1A was demonstrated by the Ala-scanning peptide series (Figure 1D). In the n-pY-c peptide background, residues at either position –2 or +3 appeared to be dispensable for binding since either could be replaced by an Ala residue without significantly compromising the affinity of the resulting peptides. Together, these observations have unambiguously identified three sites or 'prongs' in the SLAM-Tyr281 peptide that mediate high-affinity binding to SAP/SH2D1A. These prongs correspond to residues at positions –2 (Thr or Ser) and +3 (Val or Ile), and to a pTyr residue at position '0'. A combination of any two of the three prongs in a peptide is both necessary and sufficient for high-affinity SAP/SH2D1A binding.

Structural basis for the 'three-pronged' binding mode of the SAP/SH2D1A SH2 domain

In order to understand the structural basis underlying the 'three-pronged' interaction between SAP/SH2D1A and its targets, we determined its three-dimensional (3D) solution structure in complex with two distinct peptides, n-pY (RKSLTIpYA) and n-Y-c (RKSLTIYAQVQK). Peptide n-pY was selected for structural analysis because it is representative of a novel mode of ligand recognition by an SH2 domain, unique to SAP/SH2D1A. The structure of the SAP/SH2D1A–n-pY complex offers an example of how an SH2 domain recognizes a peptide devoid of the typical contacts C-terminal to the phosphotyrosine. Peptide n-Y-c was chosen for comparative purposes, although a crystal structure of the SAP/SH2D1A SH2 domain in complex with an essentially identical peptide was recently reported (Poy *et al*., 1999).

The C-terminal 25 residues of SAP/SH2D1A were unstructured in both complexes. The ^{1}H–^{15}N HSQC cross-peaks corresponding to this region of the protein were very narrow and intense, indicative of rapid and unhindered tumbling in solution (Li *et al*., 1999). Moreover, no intermediate- or long-range nuclear Overhauser effects (NOEs) could be observed beyond residue 105. Consequently, only residues 1–107, corresponding essentially to the SH2 domain region of the protein (residues 6–102), were included in the structure calculations. Figure 2 shows an overlay of the 20 lowest energy structures for each complex calculated using ARIA (Nilges *et al*., 1998), with statistics of the structures given in Table I.

As shown in Figure 3A and B, the SAP/SH2D1A SH2 domain adopts a conventional SH2 domain fold characterized by a large central β-sheet flanked by two α-helices and a small β-sheet (Cohen *et al*., 1995). In both complexes, the peptides assume an extended conformation. Amino acids N-terminal to Tyr in peptide n-Y-c or pTyr in peptide n-pY make almost identical contacts with the protein in the two complexes (Figures 2 and 3). The N-terminal 'prong', Thr-2, fits into a well-defined binding site formed by Arg13, Glu17, Ile51 and Thr53 (Figure 4). Thr-2 forms a meshwork of interactions with these residues through both hydrogen bonds and hydrophobic interactions. The main-chain carbonyl group and the side-chain hydroxyl of Thr-2 are within hydrogen-bonding distance with the side chains of Thr53 and Glu17, although the latter hydrogen bond may be mediated by a water molecule (Poy *et al*., 1999). In addition, van der Waals contacts occur between the γ-methyl group of Ile51 and C_α of Thr-2, and between side chains of Arg13 and Thr-2 (Figure 4), as demonstrated by observed NOEs. The dual polar/hydrophobic nature of interactions occurring at position –2 explains the strong preference for Thr at this position seen in the SPOTs peptide binding study.

The middle 'prong', the phosphotyrosine, is present in peptide n-pY, but absent in n-Y-c. Even though the binding pocket occupied by the Tyr/pTyr side chain is virtually the same in both complexes, the unphosphorylated Tyr is more mobile. While numerous NOEs can be

Table I. Statistics for the 20 lowest energy SAP/SH2D1A–SLAM peptide complex structures

	SAP/SH2D1A–n-pY	SAP/SH2D1A–n-Y-c
R.m.s.d. from distance restraints (Å)		
all (3157, 3950)[a]	0.0083 ± 0.0001	0.0073 ± 0.001
unambiguous (1930, 2252)[b]	0.0080 ± 0.0002	0.0078 ± 0.0009
ambiguous (1177, 1653)	0.0082 ± 0.0003	0.0045 ± 0.0003
hydrogen bonds (50, 52)	0.0104 ± 0.001	0.0198 ± 0.001
R.m.s.d. from dihedral restraints (°)		
all (171, 128)	0.157 ± 0.019	0.163 ± 0.016
Deviations from idealized geometry		
bonds (Å)	0.0011 ± 0.00002	0.0011 ± 0.00003
angles (°)	0.272 ± 0.001	0.273 ± 0.002
impropers (°)	0.138 ± 0.003	0.154 ± 0.004
Procheck Ramachandran map analysis		
most favoured regions	76.3%	79.2%
additional allowed regions	22.7%	19.8%
generously allowed regions	1.0%	1.0%
disallowed regions	0.0%	0.0%
Energy (kcal/mol)		
van der Waals (Lennard–Jones potential)	–148 ± 17	–276 ± 20
Atomic r.m.s.d. (Å) from mean structure[c]		
backbone	0.20 ± 0.05	0.29 ± 0.08
heavy	0.59 ± 0.14	0.70 ± 0.17

[a]The number of restraints for the n-pY and n-Y-c peptide complex structures, respectively, are given in parentheses.
[b]Of these restraints, 392 of 1930 for the n-pY complex and 507 of 2252 for the n-Y-c complex are structurally redundant.
[c]Superposition involved protein residues 6–102 and peptide residues –4 to +1 relative to pTyr in peptide n-pY and –4 to +5 in peptide n-Y-c.

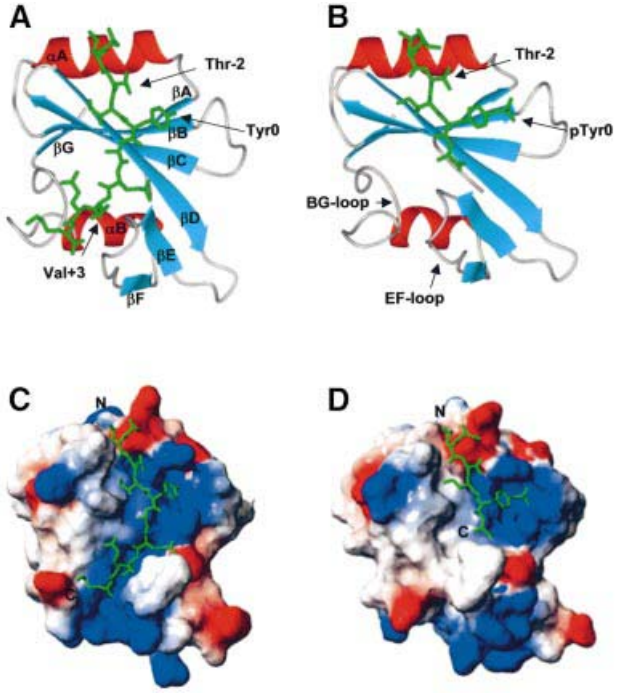

Fig. 3. Structures of the SAP/SH2D1A SH2 domain in complex with peptides n-Y-c (**A** and **C**) and n-pY (**B** and **D**). The protein is shown in ribbon representations in (A) and (B) with β-strands in cyan, α-helices in red and loops in gray, and in surface diagrams in (C) and (D) with blue indicating positive and red indicating negative electrostatic potentials. The bound peptides are in green. The secondary structural elements of the protein are labeled in (A) and (B), as are residues of the peptides important for binding. This figure was generated using MolMol (Koradi *et al*., 1996).

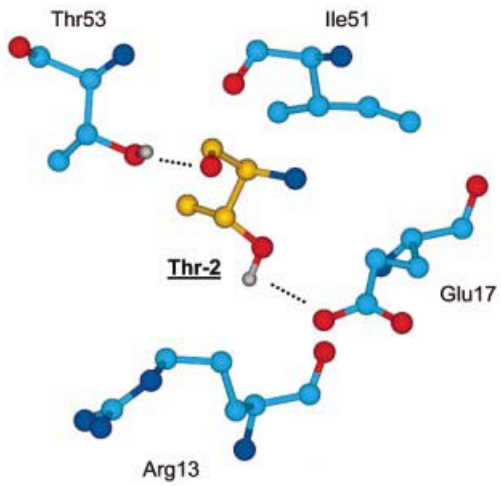

Fig. 4. Spatial orientation of residues in the SAP/SH2D1A SH2 domain (shown in cyan) involved in binding to the Thr-2 site (in gold) of the peptides. Protein resides shown are all within 4 Å of Thr-2 in both complexes. Oxygen atoms are colored red and nitrogen blue. Dashed lines indicate hydrogen-bonding interactions. Note that, except for the hydroxyls of the two Thr residues, hydrogen atoms are omitted for clarity.

observed between the pTyr ring protons of peptide n-pY and Arg13, Arg32, Val37, Val40, Cys42, Ile51, Thr53, Tyr54 and Arg55 of the protein, the Tyr residue in peptide n-Y-c shows a relatively limited number of NOE contacts with Arg13, Thr53 and Arg55. The increased rigidity of the pTyr ring is due mainly to hydrogen-bonding interactions between its phosphate group and the side chains of Arg32, Ser34, Ser36 and Arg55. The SPOTs peptide binding studies also demonstrate that the Tyr residue in peptide n-Y-c could be replaced by any of the remaining 19 amino acids without compromising its affinity for SAP/SH2D1A (Figure 1). These observations collectively suggest that the majority of the binding energy from the pTyr 'prong' is contributed by interactions to the phosphate group, not the aromatic ring.

Table II. Comparison of different SAP/SH2D1A–peptide complex structures[a] determined by X-ray crystallography[b] and NMR[c]

Complex	Backbone r.m.s.d. (Å) of SH2 domain	
	Residues 6–102	Residues 6–56
n-pY (NMR) verus n-Y-c (NMR)	1.359	0.760
Free (X-ray) verus n-pY (NMR)	0.913	0.747
pY281 (X-ray) verus n-pY (NMR)	1.218	0.848
Y281 (X-ray) verus n-Y-c (NMR)	1.069	0.606

[a]The sequence of peptideY281 in the crystal structures was VEKKSLTIYAQVQK. In pY281, the tyrosine is phosphorylated.
[b]See Poy *et al.* (1999).
[c]Average NMR structures are used.

The C-terminal 'prong', Val+3, is present in peptide n-Y-c, but absent in n-pY. It sits in a well-defined hydrophobic pocket lined by residues from the EF (Ala66, Glu67, Thr68, Ala69 and Lys74) and BG loops (Gly93 and Ile94). (The EF loop is located between strands E and F, while the BG loop is between helix B and strand G; Figure 3A and B). In the n-Y-c peptide complex, these loops adopt an open configuration in order to accommodate the C-terminal residues of the peptide (Figure 3A). In contrast, the two loops adopt a closed configuration in the n-pY complex (Figure 3B), a structure that bears a closer resemblance to the structure of the free protein determined by X-ray crystallography (Poy *et al.*, 1999) than to that of the SAP/SH2D1A–SLAM-pY281 peptide complex (Table II). The switch from an open to a closed state buries a significant amount of surface area, which otherwise would be exposed to the solvent, and closes off the portion of the peptide binding groove that would otherwise interact with the C-terminal 'prong' of the peptide. This is seen most vividly in Figure 3C and D. While the two loops in the open state allow for the formation of an elongated binding groove in the n-Y-c complex (Figure 3C), the EF loop in the SAP/SH2D1A–peptide n-pY complex closes over the cleft and, in effect, creates a ridge on the protein surface, which interacts with the truncated C-terminus of peptide n-pY (Figure 3D). The use of flexible regions of a protein, such as loops, to modify the ligand-binding surface reflects the highly adaptive nature of the SAP/SH2D1A SH2 domain employing an 'induced fit' mechanism.

Backbone amide accessibility probed by hydrogen exchange rates

The most striking differences between the NMR structures of the two complexes are found in the C-terminal half of the protein, including the EF and BG loops. As seen in Figure 2, residues 6–56 superimpose very well. However, between residues 58 and 95, the structures of the two complexes diverge, suggesting considerable conformational flexibility. To characterize the dynamics of this region further, we conducted hydrogen exchange experiments to measure the accessibility of SAP/SH2D1A backbone amides to a solvent. Exchange of most amide hydrogens with a solvent requires a substantial opening of structure. Thus, amide exchange experiments measure larger amplitude structural fluctuations over much longer time scales than conventional NMR relaxation-based techniques. Amide exchange protection factors were calculated for both complexes and the results are shown in Figure 5A. In both complexes, residues 58–95 display lower protection factors than the rest of the SAP/SH2D1A molecule, confirming the dynamic nature of this region. The loops in this region are particularly mobile and even the secondary structure elements (strands βE and βF, and helix αB) are not well protected from the solvent. Thus, multiple conformations are possible even within a single complex. The NMR structure of the SAP/SH2D1A–peptide n-Y-c complex is virtually identical to its corresponding X-ray structure for the protein core (residues 6–56), with a backbone r.m.s.d. of 0.6 Å when the two structures are superimposed (Table II). However, the r.m.s.d. increases to 1.07 Å when residues 6–102 are superimposed, again suggesting considerable conformational variability between residues 58 and 95 even though both structures are in an 'open' configuration. The differences between the NMR structures and the previously determined X-ray structures (Table II) highlight the dynamic nature of this region, which have been confirmed and quantitated by hydrogen exchange measurements (Figure 5A). Amide and methyl group relaxation experiments probing fast time scale motion have also been performed, showing behavior in agreement with the hydrogen exchange results (P.J.Finerty,Jr, D.R.Muhandiram and J.D.Forman-Kay, unpublished data).

The differences in protection factors between the SAP/SH2D1A–n-pY and –n-Y-c structures reflect differences in binding between the two complexes. In the n-pY complex, the phosphotyrosine-binding BC loop of the protein displays much higher protection factors than in the n-Y-c complex (Figure 5). This loop appears to be quite mobile in the absence of a phosphate group, despite the many indirect hydrogen bonds observed in the crystal structure of the SAP/SH2D1A SH2 domain in complex with an unphosphorylated SLAM peptide (Poy *et al.*, 1999). These observations support the notion that the unphosphorylated tyrosine in the peptide has a rather insignificant contribution to SAP/SH2D1A binding, as also suggested by the SPOTs assay and the limited number of NOEs observed. While the n-pY complex has higher protection factors in the BC loop, the n-Y-c complex displays higher protection factors for the entire C-terminal half of the protein (Figure 5B). This suggests that the binding of residues C-terminal to pTyr greatly reduces the conformational freedom present in this region, stabilizing the 'open' conformation of the EF and BG loops.

Another interesting observation from the hydrogen exchange measurements is that residues 96–102 are

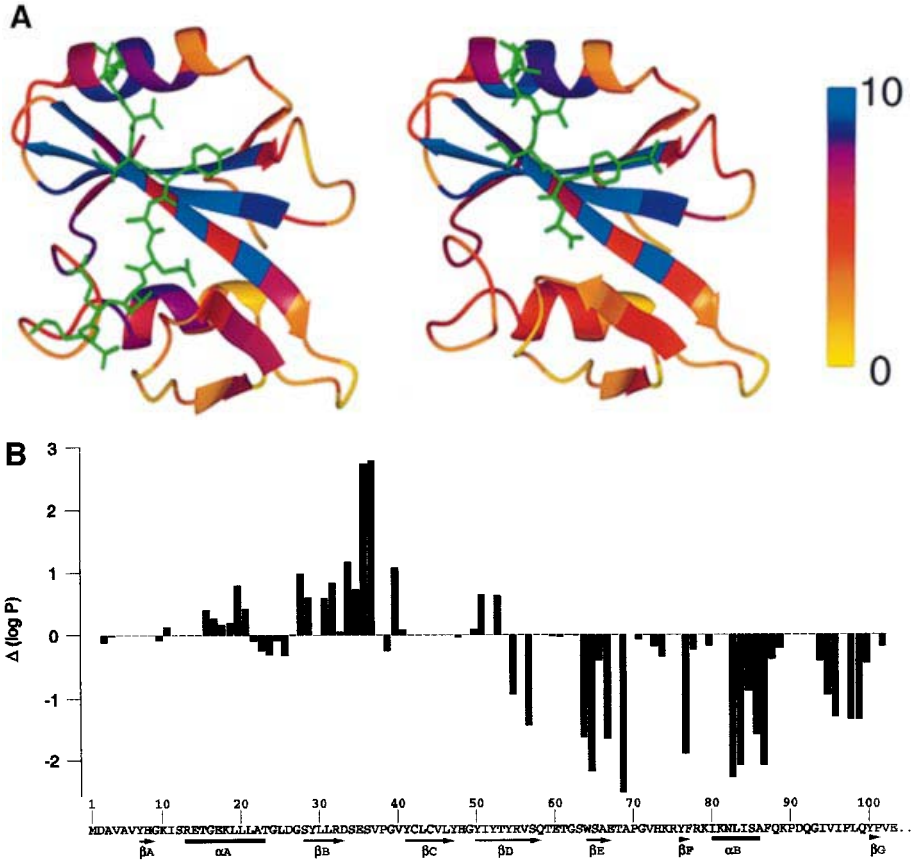

Fig. 5. (**A**) Protection factors for the SAP/SH2D1A SH2 domain in complex with peptides n-Y-c (left) and n-pY (right). Peptides are shown in green in both complexes. Residues of the protein are color coded according to their respective protection factors on a 0–10 scale (from yellow to blue with increasing protection factors). Prolines were assigned a color intermediate between those of the flanking residues. For amides with exchange rates too slow to be quantitated by CLEANEX-PM and too fast to be measured by conventional approaches, an exchange time constant of 10 s was used to calculate the protection factors. (**B**) Difference in amide protection factors between the n-pY and n-Y-c complexes as a function of residue. If quantitative data were not available for both complexes, a difference of '0' was assigned to the residue. The secondary structure is shown under the sequence of the protein.

relatively rigid (Figure 5A). It is surprising that residues 96–99 are well protected against exchange even though they are not part of any regular secondary structure element. As well, residues 100–102 form a peripheral, exposed β-strand. The high protection factors suggest that this region may be important for stabilizing the overall fold of the protein, which explains why mutations in this region compromise SAP/SH2D1A binding (see below).

Binding defects of disease-causing SAP/SH2D1A mutants

A variety of missense mutations have been identified in XLP patients. Except for the mutation ∇Tail, which changes a stop codon to an Arg and results in an addition of 11 amino acids to the C-terminus of SAP/SH2D1A (Sayos *et al*., 1998), all mutations are sequestered within the boundaries of the protein's SH2 domain. The fact that replacement of a single amino acid causes disease points to the pivotal importance of maintaining the integrity of the protein and suggests that the specificity of the SH2 domain of SAP/SH2D1A is fine-tuned for its function. Since SAP/SH2D1A binds to both phosphorylated and non-phosphorylated peptides, it is possible that the mutated proteins are defective in binding to either or both. To explore these possibilities, we generated 10 single amino acid substitution mutants according to missense mutations found in XLP patients and measured their affinities for both the phosphorylated and non-phosphorylated SLAM-Y281 peptides by fluorescence polarization. As summarized in Table III, all mutants except T53I exhibited reduced affinities for the fluorescein-labeled SLAM-pY281 peptide and all showed decreased binding to the SLAM-Y281 peptide. In addition, for the majority of mutants, binding to the non-phosphorylated SLAM peptide appeared to be more profoundly perturbed (Table III). Again, this is in accordance with the 'three-pronged' model, e.g. mutation at a single site of the protein has a less detrimental effect to binding by a peptide with three 'prongs' (e.g. SLAM-pY281) than one with only two (e.g. SLAM-Y281).

The 10 mutants can be divided into two groups according to their discrete binding behavior. Group I mutants, including Y7C, S28R, C42W, P101L and ∇Tail, displayed partially reduced affinities for both peptides compared with wild-type SAP/SH2D1A. The K_d values of the corresponding complexes of these mutants with either peptide were found to be <5 μM (Table III). Group II mutants, including R32Q, T53I, T68I, Q99P and V102G,

Table III. Relative affinity of SAP mutants for fluorescent peptides[a] SLAM-Y281 and SLAM-pY281

Protein	SLAM-Y281		SLAM-pY281	
	K_d (μM)[b]	Relative affinity (%)	K_d (μM)[b]	Relative affinity (%)
SAP	0.60 ± 0.07	100	0.26 ± 0.03	100
Y7C	2.59 ± 0.19	23	0.95 ± 0.12	27
S28R	4.19 ± 0.12	14	1.04 ± 0.09	25
C42W	2.18 ± 0.16	28	3.05 ± 0.03	9
P101L	2.57 ± 0.15	23	0.56 ± 0.06	46
∇Tail	1.08 ± 0.14	55	0.51 ± 0.04	51
R32Q	>50.0	<1	1.83 ± 0.17	14
T53I	>10.0	<6	0.25 ± 0.05	100
T68I	>150	<1	5.08 ± 1.92	5
Q99P	>100	<1	3.81 ± 0.60	7
V102G	>100	<1	2.89 ± 0.54	9

[a]The following peptides were used in the binding studies: SLAM-Y281, KSLTIYAQVAK; and SLAM-pY281, TIpYAQVAK. Both peptides were covalently labeled with fluorescein at the N-terminus via an anchor sequence KGG (Li *et al.*, 1999).
[b]K_d values given in the table are averages of at least two independent measurements.

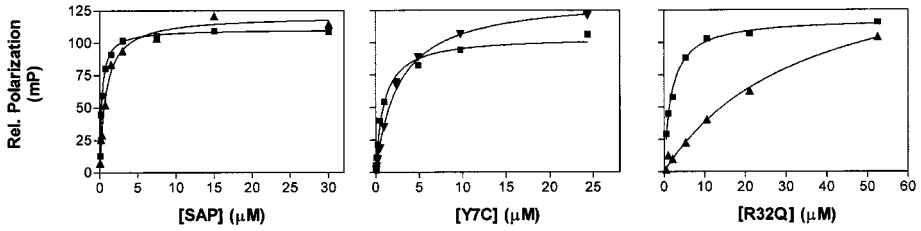

Fig. 6. Binding curves for wild-type SAP/SH2D1A and mutants Y7C and R32Q to fluorescently labeled SLAM-pY281 (squares) and SLAM-Y281 (triangles) peptides. Points representing relative fluorescence polarization values (Y) at various protein concentrations (X) from a single measurement were fitted to the equation $Y = B_{max} \times X/(K_d + X)$, where B_{max} represents maximal levels of fluorescence polarization, to yield the corresponding K_d values using the computer program Prism 3.0. Average K_d values from multiple independent measurements are given in Table III.

exhibited appreciable affinities for the SLAM-pY281 peptide (with corresponding K_d values $\leqslant$5 μM), but were incapable of binding to the SLAM-Tyr281 peptide (with corresponding K_d values >10 μM). Figure 6 shows binding curves observed for Y7C, the representative of the group I mutants, and R32Q, the representative of the group II mutants, in comparison with those for the wild-type SAP/SH2D1A protein.

Understandably, the mutation of residues directly involved in peptide recognition had a greater impact on binding than did that of residues outside of the peptide binding cleft (Figures 3 and 4). Thus, mutants R32Q, C42W, T53I and T68I all involve residues interacting with the 'prongs' of the peptide and all display markedly reduced affinity for one or both peptides. Interestingly, mutation of Thr53, a residue involved in binding to the N-terminal 'prong' Thr-2 of the peptides (Figure 4), drastically affected the affinity of mutant T53I for the SLAM-Y281 peptide, while leaving its affinity for the SLAM-pY281 peptide intact. Again, this is readily explained by the 'three-pronged' binding mechanism of SAP/SH2D1A. The presence of three 'prongs' in the SLAM-pY281 peptide makes it possible to leave out one 'prong' (e.g. Thr-2) in binding and yet maintain a high affinity for SAP/SH2D1A. This is certainly not the case for the SLAM-Y281 peptide, where only two prongs (e.g. Thr-2 and Val+3) are present. Since mutation of Thr53 is associated with XLP, this observation underscores the importance of phosphorylation-independent interaction in SAP/SH2D1A function and in the pathogenesis of XLP.

The only mutant that displays a greater affinity for the SLAM-Tyr281 peptide than for the phosphorylated peptide is C42W. Since Cys42 forms part of the binding pocket for pTyr, its replacement by a bulky Trp residue likely creates a steric clash with the phosphate group of pTyr in the SLAM-pY281 peptide. The same mutation, however, may have a less detrimental effect on binding to the less bulky Tyr residue in the SLAM-Y281 peptide.

Mutants Y7C, S28R, Q99P, P101L, V102G and ∇Tail do not involve residues at the peptide–protein interface, and their reduced affinities for both peptides are likely to be attributable to protein folding and stability. Mutant ∇Tail is extremely unstable both *in vitro* and *in vivo* (Morra *et al.*, 2001b). Surface area calculations reveal that the side chains of residues Tyr7, Gln99 and Pro101 are largely buried in both complexes, while those of Ser28 and Val102 are completely inaccessible to solvent (data not shown). Although residues Gln99, Pro101 and Val102 are not at the core of the protein, they may nonetheless be involved in stabilizing the overall fold of the protein by interacting with the protein's central β-sheet. Consistent with this, solvent exchange experiments also showed that the amide hydrogens of these residues are well protected (Figure 5).

Discussion

SH2 domains are a group of structurally conserved protein modules of ~100 amino acids, which, in general, bind selectively to phosphotyrosine-containing sequences

(Songyang *et al*., 1993; Pawson, 1995). For a typical high-affinity phosphopeptide–SH2 domain interaction, >50% of the binding free energy is derived from the pTyr residue and half of this is contributed by the charge on the phosphate group (Grucza *et al*., 1999). Naturally, exclusion of phosphotyrosine from a peptide often results in complete loss of binding affinity for conventional SH2 domains. However, this is not the case with SAP/SH2D1A.

While conventional SH2 domains bind to their cognate ligands in a 'two-pronged' mode mediated primarily by the pTyr residue and a few residues C-terminal to it (Cohen *et al*., 1995), the SAP/SH2D1A SH2 domain can interact with its ligand using a 'three-pronged' mechanism. The three prongs have been identified in the present study as residues at positions –2 and +3 relative to pTyr (or Tyr) and the pTyr residue itself. The SAP/SH2D1A SH2 domain can recognize a peptide ligand using either all three 'prongs' for maximal affinity or a combination of any two. This 'two-out-of-three-pronged' binding is clearly displayed in the solution structures of SAP/SH2D1A in complex with peptides n-pY and n-Y-c. These structures also demonstrate that each prong residue has its own well-defined binding pocket on the surface of SAP/SH2D1A.

One advantage of a 'three-pronged' binding mechanism over a 'two-pronged' one is its broader substrate specificity. For a conventional SH2 domain using the 'two-pronged' mode, pTyr binding provides the critical basal energy for peptide recognition and residues C-terminal to it confer high affinity and specificity (Grucza *et al*., 1999). Since its specificity is strictly defined by the C-terminal residues of the peptide, this SH2 domain may only bind to one type of ligand with optimal affinity. In contrast, the SAP/SH2D1A SH2 domain can employ all three prongs or engage a combination of any two for peptide/protein recognition. This versatility greatly expands the pool of potential binding partners. A Tyr-phosphorylation site in a protein can be a valid target for SAP/SH2D1A when it is either preceded by an N-terminal prong such as a Thr or Ser residue at position –2 or followed by a C-terminal prong such as a Val or Ile residue at position +3. Consistent with this possibility, SAP/SH2D1A was found to bind p62Dok, a protein that associates with the GTPase activating protein p120 Ras-GAP (Sylla *et al*., 2000). SAP/SH2D1A is capable of binding to the phosphorylated p62Dok sequence ALpY^{449}SQVQK, even though it lacks the N-terminal Thr-2 prong. Non-Tyr-containing sites that possess optimal sequences at both N- and C-termini can also, in principle, be recognized by SAP/SH2D1A. This was demonstrated in the SPOTs binding assay, in which the SAP/SH2D1A SH2 domain was found to bind to a consensus sequence $^{-2}$T/S-x-x-x-x-V/I^{+3}, which lacks a tyrosine residue.

SAP/SH2D1A has been found to bind several target proteins (Morra *et al*., 2001b) and XLP likely results from the disruption of many different interactions. The functional importance of the versatile SAP/SH2D1A SH2 domain is underscored by the various point mutations identified within this domain that are associated with XLP. A point mutation can cause a conformational change in the protein and render it unstable. Alternatively, a mutation can cause a change in specificity or a reduction in affinity of the SH2 domain for a given physiological ligand. This may be the result of steric clashes, loss of favorable interactions or changes in protein dynamics. The observation that all mutants examined in the present study displayed markedly reduced affinities for the non-phosphorylated SLAM peptide suggests that phosphorylation-independent interactions are important for proper functioning of SAP/SH2D1A and likely also for the pathogenesis of XLP. In agreement with this hypothesis, a disease-causing mutation, T53I, results in drastically reduced affinity for the unphosphorylated SLAM-Y281 peptide while retaining full capacity to bind the phosphorylated peptide.

The considerable dynamics observed in SAP/SH2D1A contribute to its ability to accommodate non-optimal sequences. Structural flexibility can improve the stability of various complexes by modulating the binding surface and by maintaining conformational entropy in the absence of favorable interactions. The flexibility of the two segments that regulate the peptide binding cleft, the BG and EF loops, allows for considerable structural plasticity, enabling the extreme versatility of binding specificity observed in this modular domain.

Materials and methods

Synthesis of peptide SPOTs on derivatized cellulose membranes

A set of undecamer SLAM-Tyr281 peptide analogs was assembled on a derivatized cellulose membrane using Auto-Spot Robot ASP 222 (Abimed, CA) according to standard solid-phase peptide synthesis chemistry. The SPOTs peptide sheet was moistened sequentially with ethanol and water prior to screening using either purified GST–SAP/SH2D1A or GST alone. Specifically, the peptide sheet was washed three times with Tris-buffered saline-T (TBS-T) buffer containing 20 mM Tris–HCl, 140 mM NaCl and 0.1% (v/v) Triton X-100 pH 7.6, and blocked with 5% skimmed milk in TBS-T for 1 h at room temperature (RT). GST–SAP/SH2D1A (~1.0 μM) or GST protein was added directly into the blocking solution and the peptide sheet was incubated at RT for an additional 1 h. The sheet was then washed three times, 5 min each, with TBS-T and once with TBS prior to addition of anti-GST antibodies. After incubation for 30 min at RT, the cellulose sheet was washed three times with TBS and developed using the ECF western blotting kit (AmershamPharmacia Biotech) following the manufacturer's recommendations and documented using a Fluor-S Multi-Imager (Bio-Rad). For re-probing, the peptide sheet was stripped by treating it sequentially with buffer A [containing 8.0 M urea, 1% (w/v) SDS and 0.5% (v/v) β-mercaptoethanol] and buffer B [containing 10% (v/v) acetic acid and 50% (v/v) ethanol], followed by several washes with deionized water.

NMR spectroscopy and structure calculation

Full-length SAP/SH2D1A (128 residues) cloned into a pET3a vector was expressed in *Escherichia coli* strain BL21(DE3) and purified as described earlier (Li *et al*., 1999) with ^{15}N or ^{13}C labeling as required. All NMR samples contained 1.0–1.5 mM protein, 20 mM sodium phosphate pH 6.0 and 100 mM NaCl, in H_2O or D_2O. Unlabeled peptides (n-pY, RKSLTIpYA amide; and n-Y-c, RKSLTIYAQVQK) were synthesized and purified as reported previously, and titrated into protein samples to form 1:1 peptide–protein complexes as monitored using HSQC spectra.

NMR experiments were carried out at 30°C on either a Varian Inova 500 or 600 MHz spectrometer equipped with *z*-axis pulsed-field gradients. Data were processed with NMRPipe (Delaglio *et al*., 1995) and analyzed with NMRView (Johnson *et al*., 1994). Backbone chemical shift assignments were obtained by analyzing CBCA(CO)NH (Grzesiek and Bax, 1992), HNCACB (Wittekind and Müller, 1993), HNCO (Kay *et al*., 1994) and (HB)CBCACO(CA)HA (Kay, 1993) spectra. Initial side-chain assignments were extracted from 3D (H)CC(CO)NH-TOCSY and H(CC)(CO)NH-TOCSY experiments (Montelione *et al*., 1992; Grzesiek *et al*., 1993), as well as 2D (Hβ)Cβ(CγCδ)Hδ and (Hβ)Cβ(CγCδCε)Hε experiments (Yamazaki *et al*., 1993) for aromatic

residues. 3D HCCH-TOCSY (Kay *et al*., 1993) and CN-NOESY (Pascal *et al*., 1994) experiments were used to further refine side-chain assignments. Stereo-specific methyl assignments for Val and Leu residues were obtained using a 10% ^{13}C-labeled sample, according to the method of Neri *et al*. (1989). Stereo-specific methylene assignments and χ_1 dihedral angles were derived using a combination of a short mixing time CN-NOESY (50 ms) and ^{3}J HNHB and HN(CO)HB experiments (Grzesiek *et al*., 1992). Peptide ^{1}H chemical shift assignments were obtained using 2D double-filtered TOCSY and NOESY (Ikura and Bax, 1992) experiments.

Distance restraints for structural calculations were obtained from CN-NOESY (50 ms and 150 ms) data and a single-filtered NOESY (200 ms; Zwahlen *et al*., 1997) for peptide–protein restraints. Note that a 200 ms mixing time was only used in the case of the intermolecular NOE experiment, which required a longer mixing time to build up appreciable intensity. In the case of the SH2 domain structure determination, the shortest mixing time for observing significant NOEs was used. Hydrogen-bonding partners were assigned based on slowly exchanging backbone amides. Dihedral angle (ϕ and ψ) restraints were calculated from chemical shifts using TALOS (Cornilescu *et al*., 1999). Manually assigned NOE restraints, dihedral angle restraints and hydrogen-bonding restraints were used as input to calculate 100 structures for each complex using CNS v.1.0 (Brünger *et al*., 1998) simulated annealing protocols. The 10 lowest energy structures were used as input structures for the automated NOE assignment program ARIA (Nilges *et al*., 1998) along with stereo-specific assignments, dihedral angle restraints, hydrogen-bonding restraints and peak lists from NOESY spectra (no manually assigned distance restraints were used as input for these calculations). A total of 100 final structures were calculated (without water) for each complex and the 20 lowest energy structures were retained. Coordinates of the energy minimized average structure for each complex have been deposited in the Protein Data Bank, accessible under code 1KA6 for the n-pY complex and 1KA7 for the n-Y-c complex.

Measurement of backbone amide proton exchange rates by NMR

Slow water–amide proton exchange rates were measured by lyophilizing an H_2O protein sample and then redissolving it in D_2O. ^{1}H–^{15}N HSQC spectra were then recorded at various time points and the decay of amide proton signals due to D_2O exchange was measured. A number of amide protons displayed no changes in peak intensity even after 6 weeks, indicating extremely slow exchange with D_2O. The fastest exchange rate measurable using this technique was that of T15 from the SAP/SH2D1A–n-pY complex, which had a time constant of 174 s. Amides that exchanged more rapidly than this disappeared too quickly to allow the acquisition of a decay curve. More rapid exchange rates were observed using a CLEANEX-PM pulse sequence, which selectively transfers magnetization from H_2O to amide groups for detection (Hwang *et al*., 1998). The slowest exchange rate that could be measured by this technique belonged to the backbone amide of D26 from the SAP/SH2D1A–n-Y-c complex, which had an exchange time constant of 5 s. The most rapid exchange rate was seen for the amide of R78, with a time constant of 0.029 s. The signal for the R78 amide is noticeably broadened in the conventional ^{1}H–^{15}N HSQC spectrum. Hence, exchange rates spanning nine orders of magnitude could be measured. Protection factors were calculated using predicted random coil exchange rates, as described by Englander and co-workers (Bai *et al*., 1993).

Generation of SAP/SH2D1A mutants and measurement of affinities for SLAM peptides

SAP/SH2D1A mutants were generated by PCR using primers incorporating the point mutations found in XLP patients and a template bearing wild-type cDNA in a pGEX4T2 vector. All mutations were confirmed by DNA sequencing. Expression and purification of the mutant proteins were carried out according to established procedures (Li *et al*., 1999). The affinities of each mutant for the phosphorylated and non-phosphorylated SLAM-Tyr281 peptides were measured by fluorescence polarization performed on a Beacon 2000 fluorescence polarization system (Panvera Co.; Li *et al*., 1997).

Acknowledgements

We thank Qin Liu for assistance in the preparation of Figure 3. This work was supported by grants from the National Cancer Institute of Canada (NCIC) to S.-C.L., J.D.F.-K. and T.P. P.M.H. is the recipient of a scholarship from the Canadian Institutes of Health Research. S.-C.L. is a Research Scientist of NCIC with funds made available by the Cancer Society of Canada. T.P. and L.E.K. are international scholars of the Howard Hughes Research Institutes.

References

Bai,Y., Milne,J.S., Mayne,L. and Englander,W.S. (1993) Primary structure effects on peptide group hydrogen exchange. *Proteins*, **17**, 75–86.

Blankenmeyer-Menge,B., Nimtz,M. and Frank,R. (1990) An efficient method for anchoring Fmoc-amino acids to hydroxyl-functionalised solid supports. *Tetrahedron Lett.*, **31**, 1701–1704.

Brünger,A.T. *et al*. (1998) Crystallography and NMR system: a new software suite for macromolecular structure determination. *Acta Crystallogr. D*, **54**, 905–921.

Cocks,B.G., Chang,C.C., Carballido,J.M., Yssel,H., de Vries,J.E. and Aversa,G. (1995) A novel receptor involved in T-cell activation. *Nature*, **376**, 260–263.

Coffey,A.J. *et al*. (1998) Host response to EBV infection in X-linked lymphoproliferative disease results from mutations in an SH2-domain encoding gene. *Nature Genet.*, **20**, 129–135.

Cohen,G.B., Ren,R. and Baltimore,D. (1995) Modular binding domains in signal transduction proteins. *Cell*, **80**, 237–248.

Cornilescu,G., Delaglio,F. and Bax,A. (1999) Protein backbone angle restraints from searching a database for chemical shift and sequence homology. *J. Biomol. NMR*, **13**, 289–302.

Delaglio,F., Grzesiek,S., Vuister,G.W., Zhu,G., Pfeifer,J. and Bax,A. (1995) NMRPipe: a multidimensional spectral processing system based on UNIX PIPES. *J. Biomol. NMR*, **6**, 277–293.

Frank,R. and Doring,R. (1988) Simultaneous multiple peptide synthesis under continuous flow conditions on cellulose paper discs as segmental solid synthesis. *Tetrahedron*, **44**, 6031–6040.

Grucza,R.A., Bradshaw,J.M., Futterer,K. and Waksman,G. (1999) SH2 domains: from structure to energetics, a dual approach to the study of structure–function relationships. *Med. Res. Rev.*, **19**, 273–293.

Grzesiek,S. and Bax,A. (1992) Correlating backbone amide and side chain resonances in larger proteins by multiple relayed triple resonance NMR. *J. Am. Chem. Soc.*, **114**, 6291–6293.

Grzesiek,S., Ikura,M., Clore,G.M., Gronenborn,A.M. and Bax,A. (1992) A 3D triple-resonance NMR technique for qualitative measurement of carbonyl-Hβ J couplings in isotopically enriched proteins. *J. Magn. Reson.*, **96**, 215–221.

Grzesiek,S., Anglister,J. and Bax,A. (1993) Correlation of backbone amide and aliphatic side-chain resonances in ^{13}C/^{15}N enriched proteins by isotropic mixing of ^{13}C magnetization. *J. Magn. Reson. B*, **101**, 114–119.

Hwang,T.-L., van Zijl,P.C.M. and Mori,S. (1998) Accurate quantitation of water–amide proton exchange rates using the phase-modulated CLEAN chemical EXchange (CLEANEX-PM) approach with a Fast-HSQC (FHSQC) detection scheme. *J. Biomol. NMR*, **11**, 221–226.

Ikura,M. and Bax,A. (1992) Isotopic-filtered 2D NMR of a protein–peptide complex: study of a skeletal muscle myosin light chain kinase fragment bound to calmodulin. *J. Am. Chem. Soc.*, **114**, 2433–2440.

Johnson,B.A. and Blevins,R.A. (1994) NMRView: a computer program for the visualization and analysis of NMR data. *J. Biomol. NMR*, **4**, 603–614.

Kay,L.E. (1993) Pulsed-field gradient-enhanced three-dimensional NMR experiments for correlating ^{13}Cα/β ^{13}C′ and ^{1}Hα chemical shifts in uniformly ^{13}C-labeled proteins dissolved in H_2O. *J. Am. Chem. Soc.*, **115**, 2055–2057.

Kay,L.E., Xu,G.-Y., Singer,A.U., Muhandiram,D.R. and Forman-Kay,J.D. (1993) A gradient enhanced HCCH-TOCSY experiment for recording side-chain ^{1}H and ^{13}C correlation in H_2O samples of proteins. *J. Magn. Reson. B*, **101**, 333–337.

Kay,L.E., Xu,G.-Y. and Yamazaki,T. (1994) Enhanced-sensitivity triple-resonance spectroscopy with minimal H_2O saturation. *J. Magn. Res. A*, **109**, 129–133.

Koradi,R., Billeter,M. and Wüthrich,K. (1996) MOLMOL, a program for display and analysis of macromolecular structures. *J. Mol. Graph.*, **14**, 51–55.

Latour,S., Gish,G., Helgason,C.D., Humphries,R.K., Pawson,T. and Veillette A. (2001) Regulation of SLAM-mediated signal transduction by SAP, the X-linked lymphoproliferative gene product. *Nature Immunol.*, **2**, 681–690.

Li,S.-C., Songyang,Z., Vincent,S.J.F., Zwahlen,C., Wiley,S., Cantley,L.,

Kay,L.E., Forman-Kay,J. and Pawson,T. (1997) High-affinity binding of the *Drosophila* Numb phosphotyrosine-binding domain to peptides containing a Gly-Pro-(p)Tyr motif. *Proc. Natl Acad. Sci. USA*, **94**, 7204–7209.

Li,S.-C., Gish,G., Yang,D., Coffey,A.J., Forman-Kay,J.D., Ernberg,I., Kay,L.E. and Pawson,T. (1999) Novel mode of ligand binding by the SH2 domain of the human XLP disease gene product SAP/SH2D1A. *Curr. Biol.*, **9**, 1355–1362.

Montelione,G.T., Lyons,B.A., Emerson,S.D. and Tashiro,M. (1992) An efficient triple resonance experiment using carbon 13 isotropic mixing for determining sequence-specific resonance assignments of isotopically-enriched proteins. *J. Am. Chem. Soc.*, **114**, 10974–10975.

Morra,M., Howie,D., Grande,M.S., Sayos,J., Wang,N., Wu,C., Engel,P. and Terhorst,C. (2001a) X-linked lymphoproliferative disease: a progressive immunodeficiency. *Annu. Rev. Immunol.*, **19**, 657–682.

Morra,M. *et al*. (2001b) Characterization of SH2D1A missense mutations identified in X-linked lymphoproliferative disease patients. *J. Biol. Chem.*, **276**, 36809–36816.

Neri,D., Szyperski,T., Otting,G., Senn,H. and Wüthrich,K. (1989) Stereospecific nuclear magnetic resonance assignments of the methyl groups of valine and leucine in the DNA-binding domain of the 434 repressor by biosynthetically directed fractional 13C labeling. *Biochemistry*, **28**, 7510–7516.

Nichols,K.E. *et al*. (1998) Inactivating mutations in an SH2 domain-encoding gene in X-linked lymphoproliferative syndrome. *Proc. Natl Acad. Sci. USA*, **95**, 13765–13770.

Nilges,M. and O'Donoghue,S.I. (1998) Ambiguous NOEs and automated NOE assignment. *Prog. NMR Spectrosc.*, **32**, 107–139.

Pascal,S.M., Muhandiram,D.R., Yamazaki,T., Forman-Kay,J.D. and Kay,L.E. (1994) Simultaneous acquisition of ^{15}N- and ^{13}C-edited NOE spectra of proteins dissolved in H_2O. *J. Magn. Reson. B*, **103**, 197–201.

Pawson,T. (1995) Protein modules and signaling networks. *Nature*, **373**, 573–580.

Poy,F., Yaffe,M.B., Sayos,J., Saxena,K., Morra,M., Sumegi,J., Cantley,L.C., Terhorst,C. and Eck,M.J. (1999) Crystal structures of the XLP protein SAP reveal a class of SH2 domains with extended, phosphotyrosine-independent sequence recognition. *Mol. Cell*, **4**, 555–561.

Purtilo,D.T., Cassel,C.K., Yang,J.P.S., Harper,R., Stephenson,S.R., Landing,B.H. and Vewter,G.F. (1975) X-linked recessive progressive combined variable immunodeficiency (Duncan's disease). *Lancet*, **1**, 935–941.

Purtilo,D.T., Bhawan,J., Hutt,L.M., De Nicola,L., Szymanski,I., Yang,J.P.S., Boto,W., Naier,R. and Thorley-Lawson,D. (1978) Epstein–Barr virus in the X-linked recessive lymphoproliferative syndrome. *Lancet*, **1**, 798–801.

Satterthwaite,A.B., Rawlings,D.J. and Witte,O.N. (1998) DSHP: a 'power bar' for sustained immune responses? *Proc. Natl Acad. Sci. USA*, **95**, 13355–13357.

Sayos,J. *et al*. (1998) The X-linked lymphoproliferative-disease gene product SAP regulates signals induced through the co-receptor SLAM. *Nature*, **395**, 462–469.

Songyang,Z. *et al*. (1993) SH2 domains recognize specific phosphopeptide sequences. *Cell*, **72**, 767–778.

Sumegi,J. *et al*. (2000) Correlation of mutations of the SH2D1A gene and Epstein–Barr virus infection with clinical phenotype and outcome in X-linked lymphoproliferative disease. *Blood*, **96**, 3118–3125.

Sylla,B.S., Murphy,K., Cahir-McFarland,E., Lane,W.S., Mosialos,G. and Kieff,E. (2000) The X-linked lymphoproliferative syndrome gene product SH2D1A associates with p62dok (Dok1) and activates NF-κB. *Proc. Natl Acad. Sci. USA*, **97**, 7470–7475.

Tangye,S.G., Lazetic,S., Woollatt,E., Sutherland,G.R., Lanier,L.L. and Phillips,J.H. (1999) Human 2B4, an activating NK cell receptor, recruits the protein tyrosine phosphatase SHP-2 and the adaptor signaling protein SAP. *J. Immunol.*, **162**, 6981–6985.

Tangye,S.G., Phillips,J.H., Lanier,L.L. and Nichols,K.E. (2000) Functional requirement for SAP in 2B4-mediated activation of human natural killer cells as revealed by the X-linked lymphoproliferative syndrome. *J. Immunol.*, **165**, 2932–2936.

Wittekind,M. and Müller,L. (1993) HNCACB, a high sensitivity 3D NMR experiment to correlate amide proton and nitrogen resonances with the α- and β-carbon resonances in proteins. *J. Magn. Reson. B*, **101**, 201–205.

Yamazaki,T., Forman-Kay,J.D. and Kay,L.E. (1993) Two-dimensional NMR experiments for correlating $^{13}C\beta$ and $^{1}H\delta/\varepsilon$ chemical shifts of aromatic residues in ^{13}C-labeled proteins via scalar couplings. *J. Am. Chem. Soc.*, **115**, 11054–11055.

Yin,L. *et al*. (1999) SH2D1A mutation analysis for diagnosis of XLP in typical and atypical patients. *Hum. Genet.*, **105**, 501–505.

Zwahlen,C., Legault,P., Vincent,S.J.F., Greenblatt,J., Konrat,R. and Kay,L.E. (1997) Methods for measurement of intermolecular NOEs by multinuclear NMR spectroscopy: application to a bacteriophage λ N-peptide/boxB RNA complex. *J. Am. Chem. Soc.*, **119**, 6711–6721.

Received September 3, 2001; revised November 14, 2001; accepted December 5, 2001